JOURNAL OF SOLID STATE CHEMISTRY 48, 49–64 (1983)

Electron Microscopic Study of Dehydration Transformations. Part III: High Resolution Observation of the Reaction Process FeOOH → Fe_2O_3*

FUMIO WATARI,† P. DELAVIGNETTE,‡ J. VAN LANDUYT, AND S. AMELINCKX§

University of Antwerp (RUCA), Groenenborgerlaan 171, B 2020 Antwerp, Belgium

Received May 14, 1982; in revised form January 14, 1983

The dehydration reaction accompanying the goethite–hematite transformation was observed by high resolution electron microscopy. The origin of the satellites which appear during the transformation is discussed from the point of view of structure factor and shape factor. Details of the transformation mechanism have been clarified through these results and from the considerations based on the observations. The transformation goes directly from goethite to hematite in such a way that the dehydration reaction is completed within a small volume of about 60 Å width in such a manner that practically only local rearrangement into the product structure takes place, growth of hematite being very limited. After surface transformation is completed, bulk transformation develops spatially by the repeated generation of units composed of voids and hematite, until the whole volume is occupied by such units. The role of the voids and the changes of their morphology are also discussed in comparison with other interpretations of the transformation sequences.

I. Introduction

The products of the dehydration reaction 2α-FeOOH → α-Fe_2O_3 + H_2O (*1, 2*) are characterized in several ways by their diffraction effects. The agglomeration of small twinned hematite crystallites formed as a result of the topotactic transformation (*3*) gives rise to a "mosaic structure" in electron diffraction for which usually dynamical conditions prevail (*4*). Periodic arrays of pairs of voids and hematite crystallites give rise to a small angle diffraction effect (*5, 6*). This was previously interpreted in a different way (*1*).

The present paper will deal with the transformation mechanism which leads to characteristic products described above as studied by means of high resolution electron microscopy. The details of the experimental procedure are described elsewhere (*4*).

* Work performed under the auspices of the associations RUCA-SCK and CEN-IRE-ULB. Financial support of IIKW-NFWO is acknowledged.

† Present address: Research Institute for Scientific measurements, Tohoku University, 2-1-1 Katahira, Sendai 980, Japan.

‡ C.E.N.-S.C.K., B 2400-MOL, Belgium.

§ Also at C.E.N.-S.C.K., B 2400-MOL, Belgium.

2. Observations

2.1. General Expression of the Orientation Relationship

Figure 1 represents the diffraction patterns of goethite during transformation into

0022-4596/83 $3.00

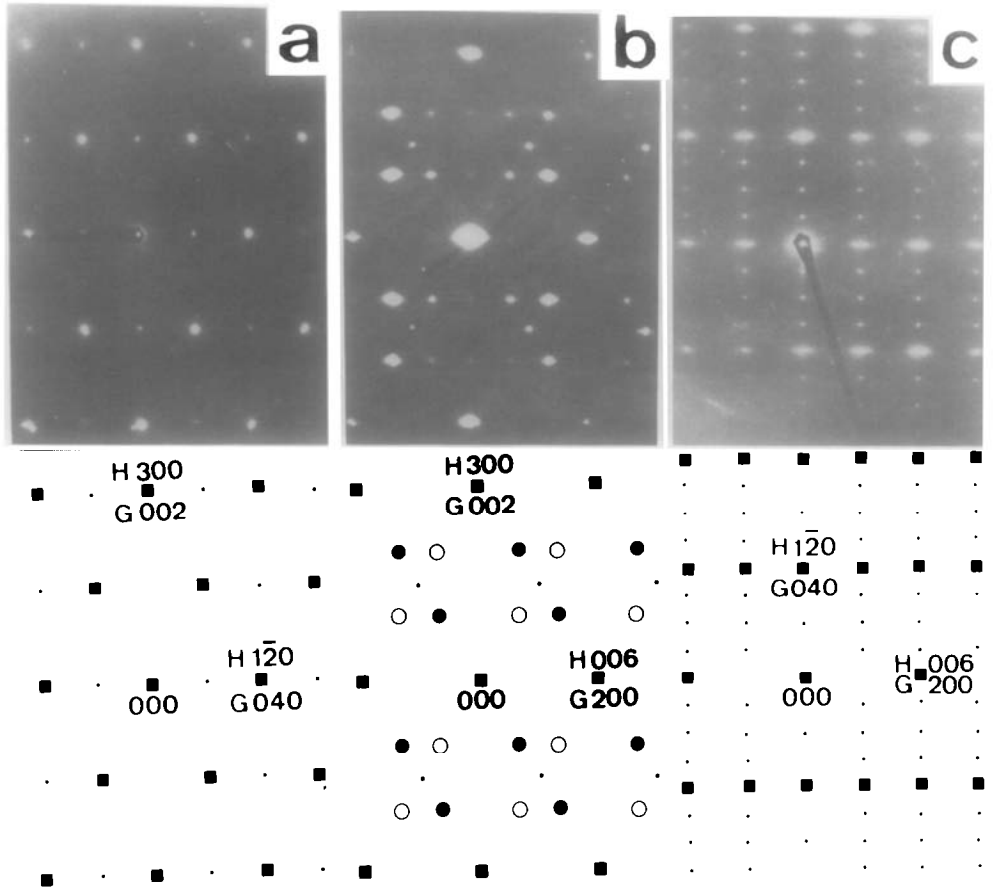

FIG. 1. Diffraction patterns during transformation in three principal orientations of goethite. Both goethite and hematite spots are observable. The three orientations are (a) G[100]//H[001]; (b) G[010]// H[010]; (c) G[001]//H[210]. The symbols mean · goethite; ● hematite obverse; ○ hematite reverse; ■ spots common to goethite, hematite obverse and reverse.

hematite in its three principal orientations. Both goethite and hematite spots are observed. On these diffraction patterns one can see several features characterizing the transformation. Satellites appear around hematite spots along a line perpendicular to H(001)[1] planes. This is due to small angle diffraction from a periodic texture (*5*).

Among the basic spots, those of goethite are sharp while the hematite spots are broadened in all diffraction patterns. The diffraction pattern in the G[010]//H[010] orientation (Fig. 1b) shows that hematite is composed of two rhombohedral twins (*1*), obverse and reverse (*7*). The difference in intensity of the hematite spots is clearly recognizable. These features are explained by the mosaic texture in electron diffraction due to twinned crystallite formation (*4*).

Among the hematite reflections (*hkl*), those for which l or $h-k$ are not multiples of three belong either to obverse or to reverse hematite. When l and $h-k$ are multiples of three, they are common to both hematite twins and goethite (*4*). This causes a

[1] The Miller (three) indices system is also used throughout for the hexagonal lattice.

different size effect in the X-ray diffraction peak widths (*8, 9*).

The features described above are mainly due to the morphological effect of the product. Between the structure of the starting and product materials the following orientation relationship can be deduced from Fig. 1.

For planes of goethite (G($h_G k_G l_G$) and hematite H($h_H k_H l_H$)

$$h_H = k_G/4 + 3l_G/2$$
$$k_H = -k_G/2$$
$$l_H = 3h_G.$$

For directions G[$u_G v_G w_G$) and H[$u_H v_H w_H$]

$$u_H = 2w_G/3$$
$$v_H = -2v_G + w_G/3$$
$$w_H = u_G/3.$$

These relations can, of course, also be expressed in the hexagonal four indices system and in the rhombohedral system for hematite using the appropriate transformation matrices (*7*). The mean reason for the simplicity of these expressions is the very small misfit between the lattices of goethite and hematite.

It is to be noted (*4*) that the G[010]// H[010] orientation (Fig. 1b) is suitable for the observation of twin occurrence in hematite since the diffraction spots with both $l = 3n$ and $1 \neq 3n$ exist in it but not in the other two, whereas the G[001]/H[210] orientation (Fig. 1c) is the most favorable one to represent the crystal structures by high resolution electron microscopy. In both orientations satellites can be observed. Hence they are the most informative with respect to the characteristics of the reaction; in the following investigations we mainly use as specimen the cleavage fragments with the plane normal to these orientations.

2.2. Initiation of the Transformation at the Surface and in the Bulk

Very careful control of beam heating leads to the formation of moiré fringes in two directions and with a spacing equal to three times the G(101) interlayer spacing (= 3 × 2.52 Å) in specimens with the G[010]// H[010] orientation (Fig. 2a). These moiré fringes are formed by the interference between the G(101) and H(102) diffracted beams, shown schematically as type I interface in Fig. 2b for the diffraction pattern and in Fig. 3 for the image. In practice, a larger objective aperture than the one shown in Fig. 2b was used to obtain the G(101) lattice fringes in Fig. 2a. The difference of these interplanar spacings is about $\frac{1}{2}$ G(101) = $\frac{1}{3}$H(102) = 1.25 Å (Fig. 1b). The two fringe directions result from the formation of hematite in the two twinned orientations. A close look at Fig. 2a reveals that the moiré fringes in the two directions scarcely overlap each other except for the possible contributions from thin wedges at the upper and lower surfaces of the specimen. The moiré fringes formed by the overlap of the two twin related hematite crystallites exhibit a different pattern (type 3 of Figs. 2b and 3). It is therefore possible to conclude that along the beam direction there exists in general only one hematite crystallite with either orientation.

The size of a hematite crystallite along the plane H($1\bar{2}0$)//G(010) normal to the beam is, on the average, equal to five times the moiré fringe spacing = 15 × G(101), which is about 40 Å. The depth of the surface hematite layer is supposed to be of about the same order of magnitude or somewhat smaller as suggested by the results of the observations on bulk transformations (Figs. 2b and 4).

On continued heating after completion of the surface transformation, bulk transformation starts and develops. In Fig. 2b one can see that voids are formed parallel to the

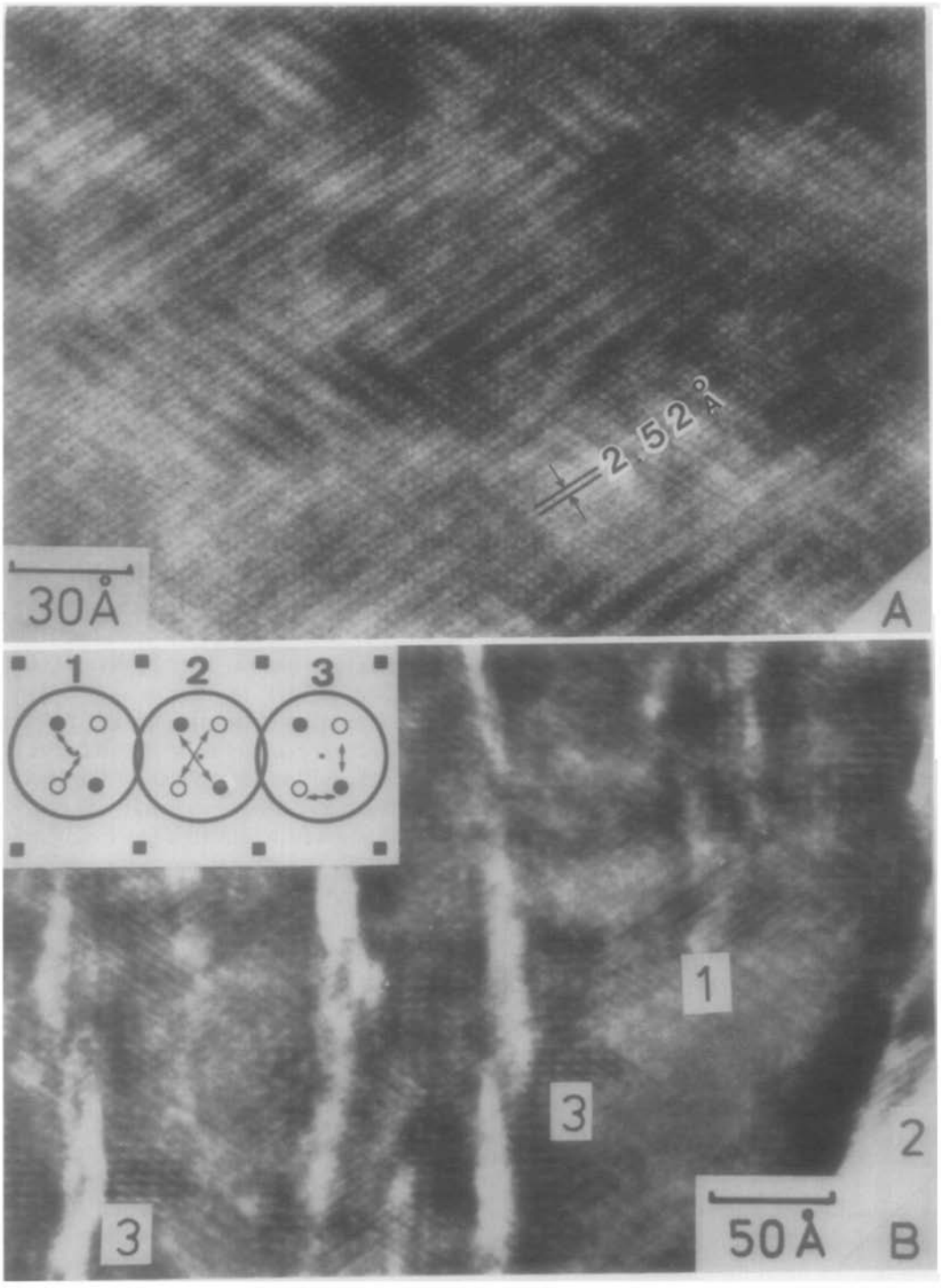

FIG. 2. Various moiré fringes during transformation observed along the G[010]//H[010] orientation. (a) resulting from the interference of beams diffracted by surface hematite and matrix goethite. The moiré fringes appear every three G(101) lattice fringes (= 2.52 Å). (b) produced by interference of beams from surface hematite and matrix goethite (type 1), lattice fringes of hematite of either twin (type 2), and interferences of obverse and reverse hematite crystallites (type 3). Note that bulk transformation has been initiated.

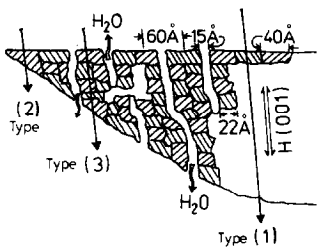

FIG. 3. Schematic explanation of the transformation mechanism. Values inside are typical averages just after transformation in vacuum. Areas hatched in different directions represent twins of hematite and the part without hatches represent voids. For the types of moiré patterns we refer to Fig. 2b. The right part of the drawing represents the untransformed goethite.

G(100) = H(003) planes. They have a white contrast in the underfocused bright field image (BF) as shown in the thin part of the specimen. Note that hematite is formed on both sides of the void at the same time. Voids and hematite are always associated. Moiré patterns composed of perpendicular fringes caused by interference of type 3 shown in the inset of Fig. 2b imply that twin crystallites of hematite overlap along the beam direction. This situation is illustrated in Fig. 3.

The width of the voids along the H[001] direction is, on the average, equal to 2.5 × moiré fringe spacing H(002) which is about 17 Å, and that of a hematite crystallite layer on one side of a void is about 3.5 × H(002) = 24 Å. The total width of one unit of the sequence hematite/void/hematite is about

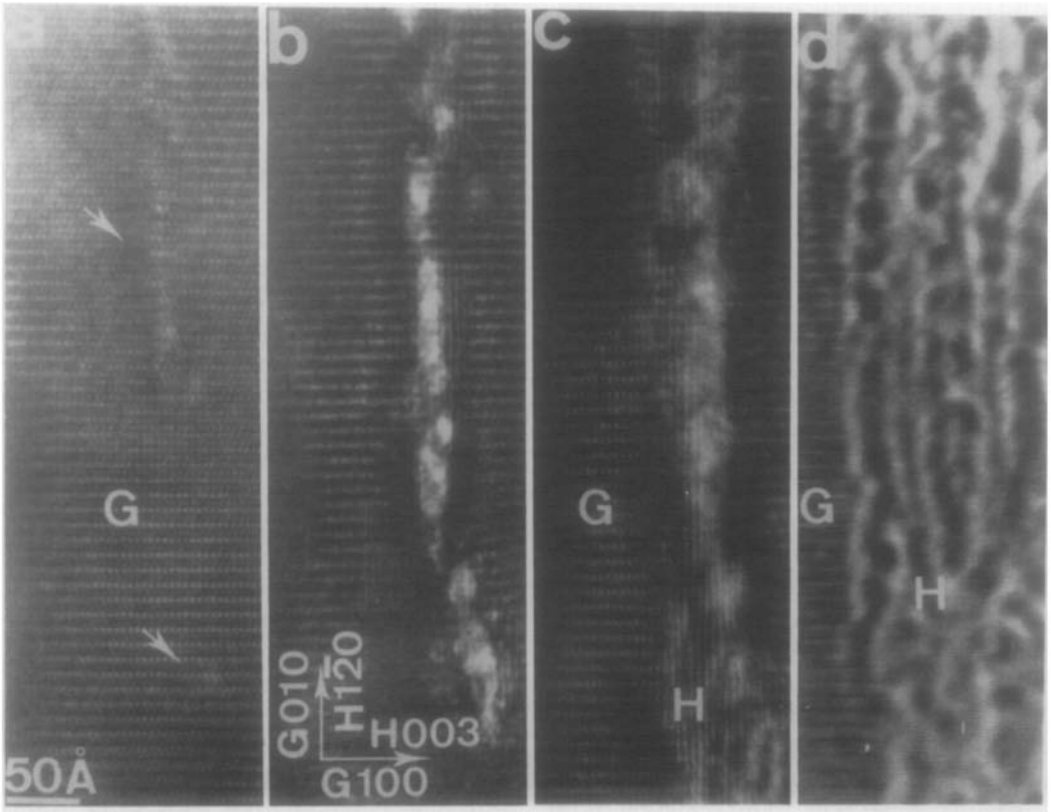

FIG. 4. Progress of bulk transformation (G[001]//H[210] orientation). (a) initiation of void formation; (b) void–hematite pairs develop along G(100) = H(003) planes; (c) and (d) further development. (a) to (c) are underfocused bright field images (BF), (d) is an overfocused BF by tilted illumination. Note that the transformation product "void–hematite" are always associated.

$17 + 2 \times 24 = 65$ Å. The ratio of void volume to the total volume of such a unit is roughly equal to the value 1:4, which is also the ratio of the loss of oxygen atoms expected from the completion of the reaction $2FeOOH \rightarrow Fe_2O_3 + H_2O$. It should be noted that the crystalline volume of both goethite and hematite is chiefly constituted by the framework of O^{2-} ions (*10*). This void–hematite pair is the smallest spatial unit of dehydration product in areas where the reaction is completed. Once this unit is formed, the size of the voids and of the hematite particles remains nearly the same under the same heating conditions.

Besides the moiré fringes formed by the interference of beams diffracted by goethite and hematite (type 1) and by two twinned hematite crystallites (type 3), genuine lattice fringes of H(102) 3.68 Å of either twin crystallite (type 2) can be observed only at the specimen edges (see Figs. 2b and 3 together). The size of a hematite crystallite along the beam direction is thus suggested to be as small as that along the G(010)//H($1\bar{2}0$) planes which are perpendicular to the beam. This is confirmed by high resolution observations of the crystal along the G[100]//H[001] orientation (Fig. 1a). It provides a perpendicular view of the void–hematite unit such as shown in Fig. 2b and the size of each crystallite is estimated to be about 25 Å.

2.3. Bulk Transformation

In Fig. 2b we saw how the bulk transformation starts in the G[010]//H[010] orientation. In Fig. 4 we follow the manner in which the spatial development of the bulk transformation proceeds in a time sequence taken under high resolution conditions, as observed along the G[001]//H[210] direction. In Fig. 4a we can observe the very beginning of the bulk transformation at the sites indicated by arrows. The initial parts of the voids under formation have a slightly brighter contrast. In Fig. 4b the formation of a void–hematite unit is already clearly observed, where the hematite part around the void is distinguished from goethite by its different lattice fringe pattern with H(003) spacing. Under these observation conditions, the relative widths of void and hematite regions appear variable, but on the average the ratio is consistent with the one derived from the G[010]//H[010] images (Fig. 2b).

The transformation develops quickly by the growth of this unit parallel to the G(100) = H(003) plane (Fig. 4a–c) and slowly in the direction perpendicular to the G(100) = H(003) plane (Fig. 4c,d), by creating new void–hematite units adjacent to the old ones.

A larger magnification of a region like Fig. 4d is shown in Fig. 5a and its dark field image (DF) in Fig. 5b. The voids in a very thin part of the specimen (< 100 Å) show a dark contrast under the diffraction conditions used here, both in an overfocused BF taken in a tilted beam illumination (Figs. 4d and 5a) and in a DF image of Fig. 5b. The last remaining part of goethite inside a hematite region is identified by its G(010) fringes (9.937 Å), which exhibit a different contrast every fourth fringe of the H($1\bar{2}0$) fringes with a spacing of 2.51 Å. In Fig. 5b G(100) and H(003) lattice fringes cannot be distinguished because of the very small misfit between them; however, the lattice fringes in the hematite region are often nonstraight because of differences in thickness as a result of the presence of voids. The lattice fringes seem to indicate that there is no serious incoherency or gap at the boundary between goethite and hematite.

On lower magnification images of a specimen observed along the G[010]//H[010] zone during transformation, the transformation zone is striated (see Fig. 1 of Ref. (*5*)). The reaction front causes the transformed area to adopt a leaf shape. This results from different growth speeds in the direction parallel and perpendicular to the

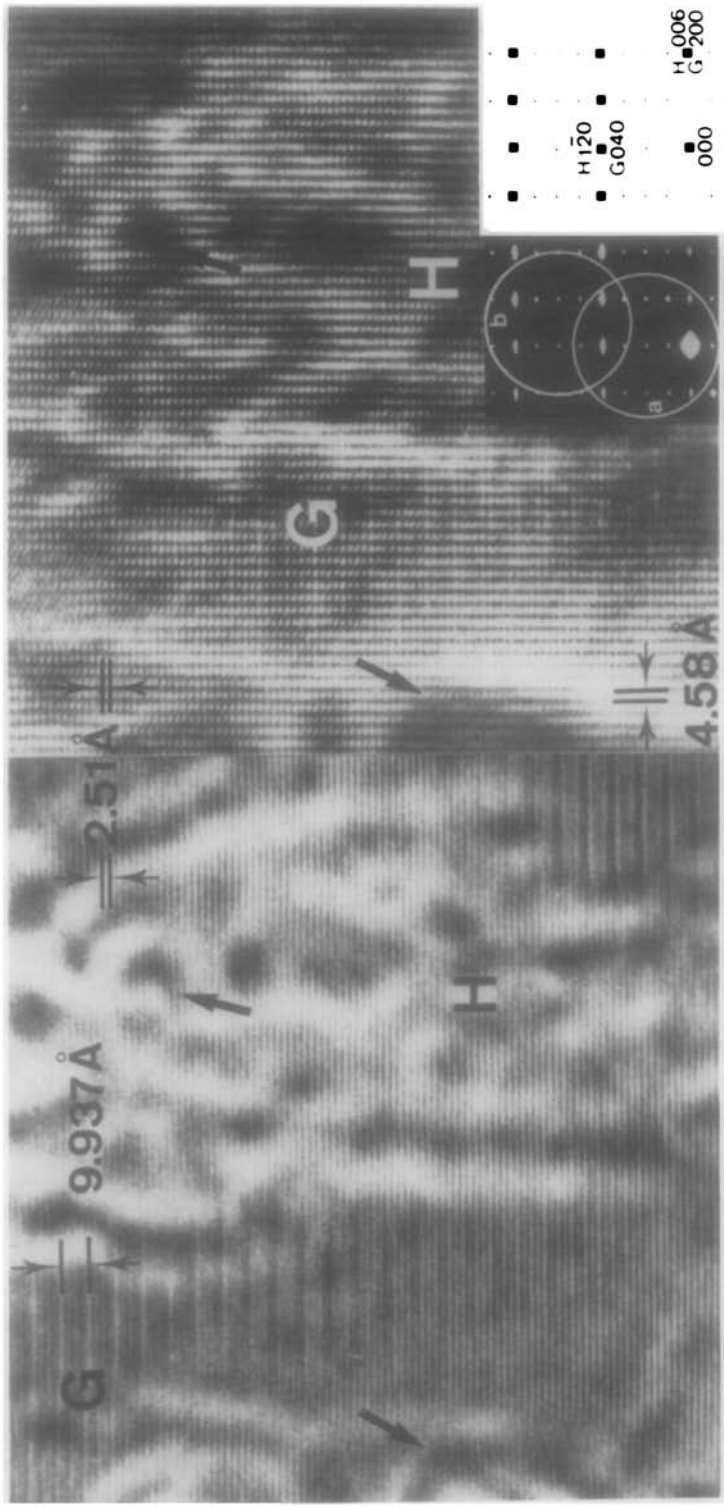

FIG. 5. High resolution images of largely transformed region observed along the G[001]//H[210] orientation. (a) overfocused bright field (BF) image in tilted illumination; (b) dark field image. The configuration of diffraction spots selected for imaging is shown in the inset. G(010) fringes appear every four layers of the H(1$\bar{2}$0) fringes.

H(003) = G(100) plane, as observed in Fig. 4.

2.4. *Recrystallization of Hematite*

After the whole area is transformed, recrystallization occurs and grain growth proceeds on continued heating. Figure 6 is a high resolution image of an area which was completely transformed into hematite. Figure 6a and b are taken from the same area carefully maintained under the same diffraction conditions. To help the reader compare successive stages in the development of the same area, corresponding points have been indicated in the two photographs by fiducial marks.

From the fringe patterns, which are similar to those shown in Fig. 2b, regions which belong to one or the other of the twin orientation (type 2), as well as regions of overlap (type 3), can be recognized. Figure 6b looks much simpler that Fig. 6a as a result of further grain growth of the crystallites. Comparison in detail reveals that the size of the crystallites of either twin, which is recognised with H(102) lattice fringes, has grown larger and that the overlapping regions of both twins identified with two perpendicular moiré fringes have shrunk, resulting in their limits becoming sharper and better defined between the two exposures.

A series of reaction stages starting from a single crystal goethite viewed along the G[001] orientation is shown in Fig. 7. Goethite (α-FeOOH) transforms into hematite (α-Fe_2O_3) by the dehydration reaction, forming a regular periodic texture (Fig. 7a). The whole is transformed except for the last part of the goethite which is identified by means of the G(010) fringes (Fig. 7b). After transformation, growth of hematite and of voids occurs by surface diffusion and coalescence (Fig. 7b,c). Figure 7d represents the same area after hematite is transformed to magnetite (Fe_3O_4) by reduction. The last reaction occurred by a strong beam heating on the specimen mounted on a carbon film in the electron microscope. Note the change of void morphology and the influence of the periodic texture on the shape of the pores in the following stages (Fig. 7c,d).

2.5. *Effect of Blocking the Dehydration*

To confirm the escape of water molecules and see the effect of a partial pressure of water vapor, carbon was evaporated on a goethite crystal with G[001] orientation to cover both upper and lower surfaces. As in the normal case, an initial void parallel to the G(100) = H(003) planes is formed at first but does not develop in spite of strong heating. Instead the voids swell and their shape becomes spherical like that of bubbles (see the white contrast part in BF (Fig. 8a) and the black contrast in DF (Fig. 8b)). It is easily recognized that the size of the voids and of the hematite regions formed around the voids (the white contrasted area without fringes in Fig. 8b) is much larger than in the periodic texture. The size and shape of the voids is the result of an internal pressure of heated water vapor which is produced by the dehydration reaction and is prevented from escaping. The larger size of the product crystallites in the presence of moisture is in accordance with the results obtained by other methods (*11, 12*).

On the other hand, goethite (region exhibiting G(010) fringes) remains stable when it is surrounded with hematite and its surface covered with a carbon film. When the carbon film happened to become partly broken so that dehydration was no longer obstructed, a regular periodic texture formed rapidly, producing small crystallites of hematite as in the normal case.

3. Discussion

3.1. *Explanation of Satellites by Structure Factor and Shape Factor*

A typical question arising in the interpretation of the transformation mechanism is

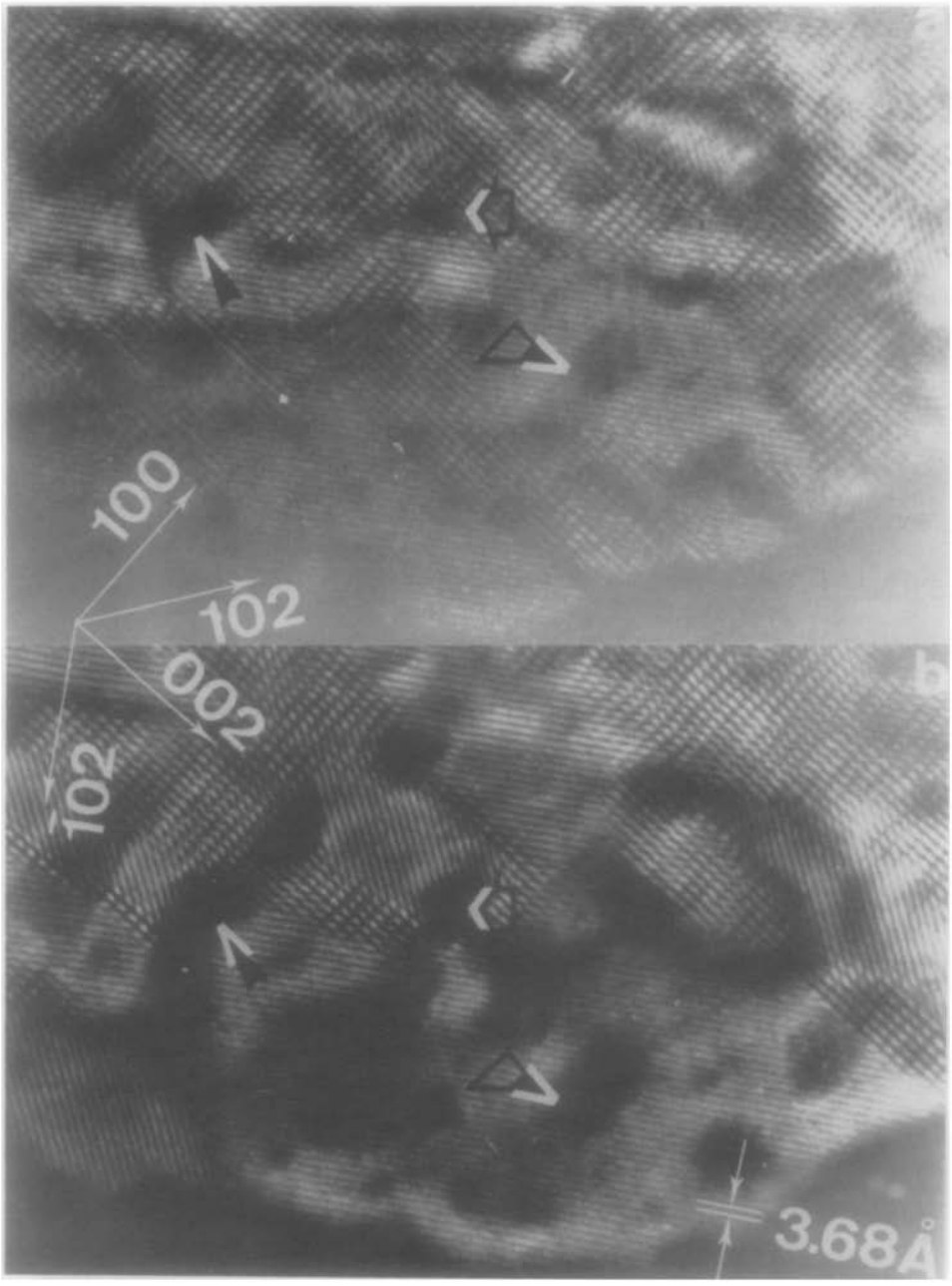

FIG. 6. Grain growth of hematite. Note the increase of the hematite crystallite size identified by means of H(102) fringes (3.68 Å).

whether the dehydration and the hematite formation occur in separate places or are closely associated in a small volume. The problem is closely related to the interpretation of the origin of the satellites which appear during transformation. To solve this

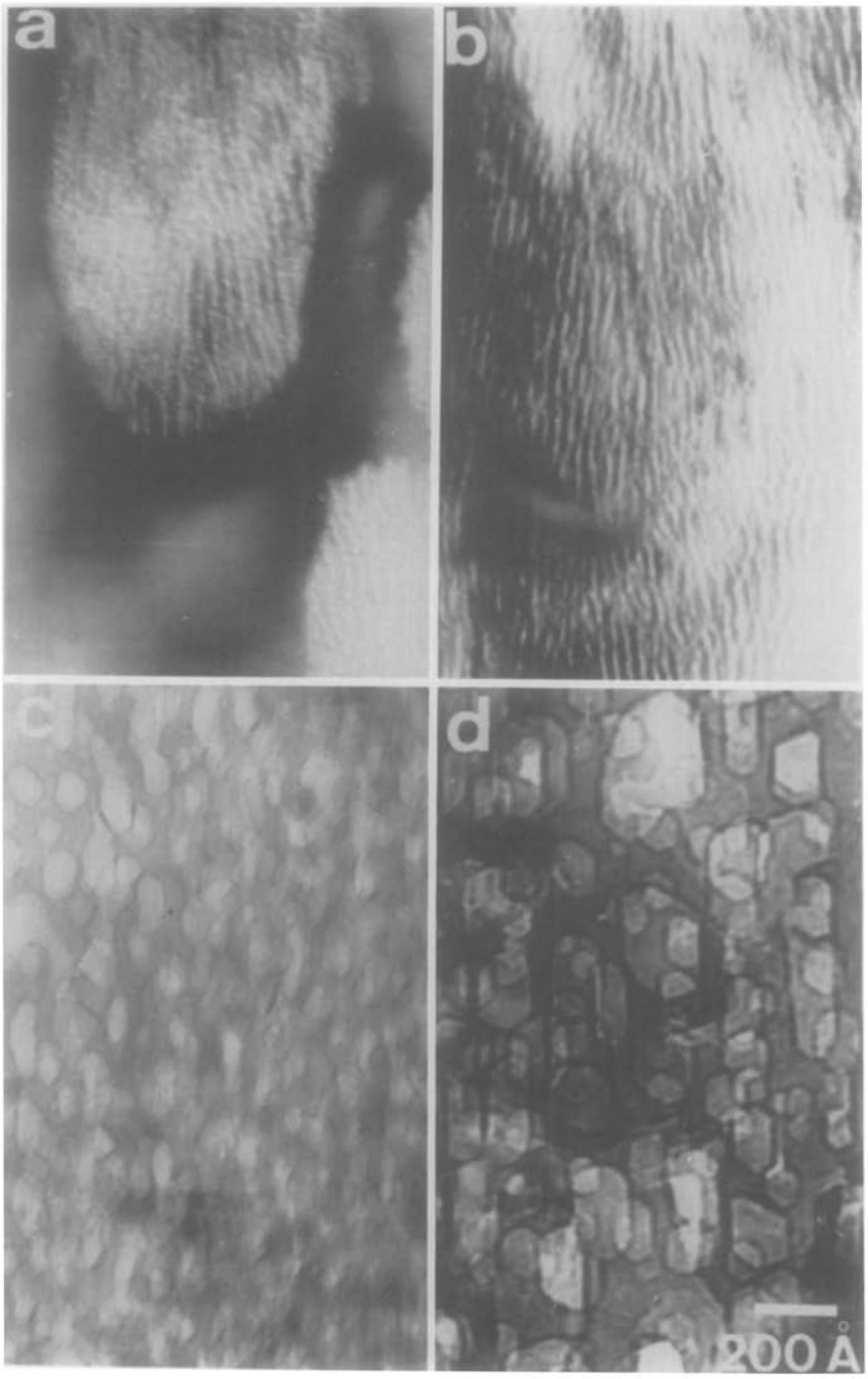

FIG. 7. Changes of void morphology. (a) periodic texture develops; (b) the dehydration reaction is almost completed; (c) after further heating; (d) after hematite is reduced to magnetite.

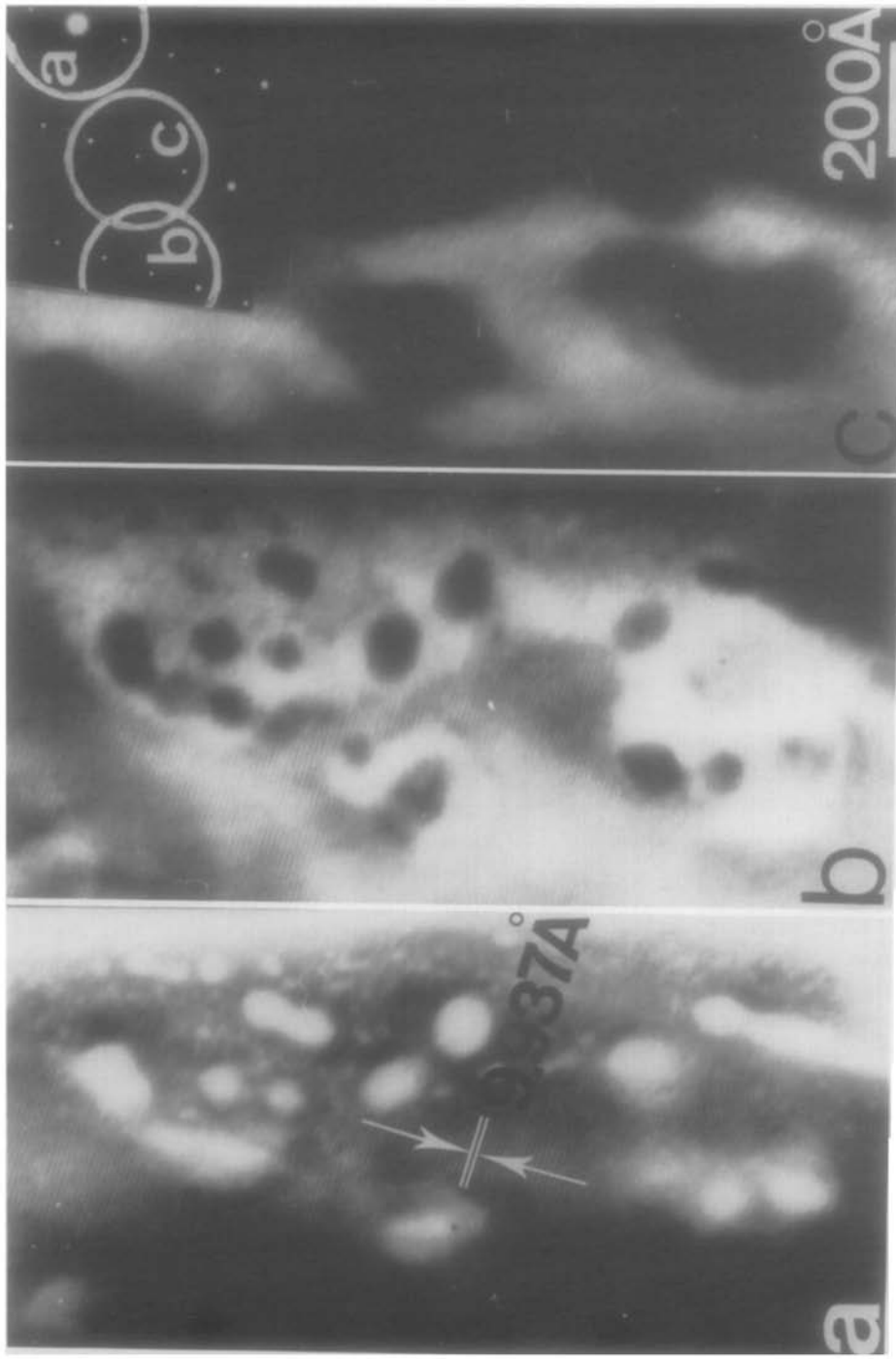

FIG. 8. Effect of blocking of the dehydration process by carbon deposition. (a) BF image; (b) DF image in goethite + hematite; (c) DF image in goethite alone. Region exhibiting lattice fringes is goethite. Note the shape and size of the void and surrounding hematite, which is quite different from a periodic texture.

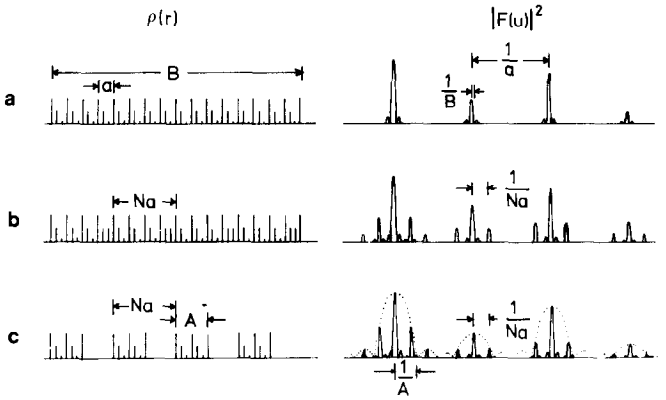

FIG. 9. Interpretation of satellites by superstructures (b) and regular periodic texture (c), both of which are the derivatives from a basic crystal (a).

problem it is first necessary to state it clearly, although it was discussed to some extent in Part II (*5*).

The intensity I diffracted by a finite volume under kinematical conditions (*13*) is proportional to the square of the amplitude of the scattering factor of the target $F(\mathbf{u})$

$$I \propto |F(\mathbf{u})|^2 \tag{1}$$

where $\mathbf{u}$ is the reciprocal space vector. The electron density distribution in real space $\rho(\mathbf{r})$ is expressed in terms of the real space vector $\mathbf{r}$ as

$$\rho(\mathbf{r}) = \rho'(\mathbf{r})s(\mathbf{r}) \tag{2}$$

where $\rho'(\mathbf{r})$ represents the electron density distribution in a volume of infinite size and $s(\mathbf{r})$ restricts this volume to a finite size. Since $F(\mathbf{u})$ is the Fourier transform of $\rho(\mathbf{r})$, it can be written as a convolution product of the form factor of an infinite crystal $F'(\mathbf{u})$ and the shape factor S($\mathbf{u}$), so that

$$F(\mathbf{u}) = F'(\mathbf{u}) * S(\mathbf{u}). \tag{3}$$

The $F'(\mathbf{u})$ can be separated into the contribution from a unit cell $F_o(\mathbf{u})$ and that resulting from the repetition of a unit cell represented by a delta function

$$\begin{aligned} F'(\mathbf{u}) &= F_o(\mathbf{u})\Sigma\delta\ (\mathbf{u} - \mathbf{ha}^*) \\ &= F_{\mathbf{h}}\ \delta(\mathbf{u} - \mathbf{ha}^*) \end{aligned} \tag{4}$$

where $\mathbf{h}$ represents (hkl) and $\mathbf{a}^*$ represents the unit vector in the reciprocal lattice ($\mathbf{a}^*\mathbf{b}^*\mathbf{c}^*$). The structure factor $F_{\mathbf{h}}$ is written using an atomic scattering factor f_i as

$$F_{\mathbf{h}} = F_{hkl} = \Sigma f_i \exp(2\pi\, i\mathbf{hr}). \tag{5}$$

(*a*) *Basic crystal with a finite size.* The electron density distribution of an ordinary crystal with a finite size, such as a single crystal particle obtained by crushing a larger single crystal of hematite, is shown schematically as a one-dimensional model in Fig. 9a where the unit cell size is a and the external size of the crystal B. In the following we shall discuss this one-dimensional model for simplicity; this does not essentially change the resulting conclusion. The shape factor is expressed as

$$S(u) = B\ \sin(\pi Bu)/\pi Bu. \tag{6}$$

The scattering factor is

$$\begin{aligned} F(u) = \Sigma F_h\delta(u \\ -ha^*) * B\ \sin(\pi Bu)/\pi Bu. \end{aligned} \tag{7}$$

The diffracted intensity $|F(u)|^2$ is shown in Fig. 9a. The diffraction peaks appear with an interval of $1:a$ with the intensity determined by F_h. The effect of the shape factor is usually negligible because $1/B \geqslant 1/a$, and the subpeaks are very weak as a result.

(*b*) *Superstructure*. A first type of derivative, from the basic crystal described above, called "superstructure" results from a change in unit cell size due to the change of atomic species, atomic positions, and number of atoms. Consequently, the unit cell size increases to Na (Fig. 9b), and the structure factor in Eq. (5) changes to F_s^h while the shape factor remains the same as in Eq. (6). The scattering factor is then

$$F^s(u) = \Sigma F_h^s \delta(u - ha^*/N) * B \sin(\pi Bu)/\pi Bu. \quad (8)$$

Its intensity profile is shown in Fig. 9b; satellites appear with a separation of $1/Na$.

(*c*) *Texture* (*regular periodic texture*). Another type of derivative, called "regular periodic texture," is related to the morphology of the specimen. Figure 9c shows the situation where the crystal structure in a unit cell is not changed, i.e., the structure factor F_h and the form factor for an infinite crystal $F'(u)$ are the same as in the original one, but the effect of a finite size of the crystallites is taken into account. In particular, the crystal volume with width A is arrayed periodically with a period Na (this may be called regular periodic texture (*5, 6*) as in Fig. 9c, then

$$S(u) = A \sin(\pi Au)/\pi Au \delta(u - ha^*/N) * B \sin(\pi Bu)/\pi Bu \quad (9)$$

and so

$$F(u) = \Sigma F_h \delta(u - ha^*) * [A \sin(\pi Au)/\pi Au \cdot \delta(u - ha^*/N) * B \sin(\pi Bu)/\pi Bu]. \quad (10)$$

The intensity profile of the diffracted beam is shown in Fig. 9c; there are satellites with a period of $1/Na$.

The intensity profiles for derivatives (b) and (c) are so similar that they cannot be distinguished on a diffraction pattern alone. Although the satellites in case (c) usually tend to scatter because of the less regular periodicity, this is not a decisive factor by which to judge the origin of the satellites. High resolution electron microscopy is essential to solve this problem. In the present case, the transformed region exhibits striae when imaged at medium resolution; it has an aspect similar to that of a superstructure. However, at high resolution no superstructure fringes are observed; instead one finds a periodic array of voids and hematite (Figs. 2b and 4). DF images of goethite and hematite are complementary; no third phase is recognized. Thus it is concluded that the striated region is a final product of the reaction. The regular periodic texture is the origin of the satellites (case (c)). If the texture is much more random, the diffraction pattern exhibits halos instead of satellites. This is the case in corundum (α-Al_2O_3) produced under electron irradiation from a diaspore crystal (α-AlOOH); the system diaspore corundum is isostructural with the present one (*5, 6*).

3.2. Transformation Mechanism

The above considerations lead us to conclude that the reaction occurs in a direct way without the formation of an intermediate phase: α-FeOOH → α-Fe_2O_3. Spatially this reaction is completed in each small volume of about 60 Å width parallel to the basal plane of the hexagonal close packed oxygen array (G(200) = H(006) plane). The volume decrease due to loss of water molecules reaches already nearly 100% of the expected value in this local volume as examined in detail in Figs. 2b and 4.

The product hematite, formed adjacent to the surface whether it is an external surface (Fig. 2) or a newly created void surface (Figs. 2, 4), consists of a layer which is only one crystallite thick and contains the two varieties in twin relation (see Fig. 3). This is revealed by the pattern of moiré fringes and in the DF image using a spot of either twin crystallite that is a spot with $l \neq 3n$.

After the hematite crystals are formed, no further noticeable growth is observed.

The transformation process consists almost exclusively of nucleation and not of nucleation and growth, where under the term nucleation we understand a process whereby islands of hematite are formed by local rearrangement of the iron atoms into the product structure. This type of mechanism without long range diffusion ws proposed for the dehydration reaction $Cd(OH_2) \rightarrow CdO + H_2O$ by Niepce *et al.* (*11*, *12*). The reason no subsequent growth takes place is probably because the diffusivity of hydrogen or Fe^{3+} in bulk hematite at the transformation temperature is very small, and once hematite is formed at the surface of goethite, the dehydration from the enclosed goethite is no longer possible. Accordingly, the formation of hematite stops immediately after nucleation.

When the diffraction patterns in Fig. 1 are compared, intensity differences among hematite are noticeable only in the G[010]// H[010] orientation (Fig. 1b), where hematite spots of both twin orientation with $l \neq 3n$ exists. The relative intensities are in accordance with the calculated structure factors under kinematical conditions (*4*). In the orientations where only hematite spots common to both twins ($l = 3n$) appear (Fig. 1a,c), the differences in intensity are not clear. The situation has a more dynamical character. It suggests that the mosaic block size of the product hematite looks larger when observed in common spots than when observed in spots belonging to one twin (*4*). This phenomenon is more clearly observed in the peak width behavior of X-ray diffractograms (*8*, *9*). The product behaves like a single crystal in common reflections and as an agglomerate composed of broken-up twin crystallites in reflections belonging to either twin. This suggests that the twin boundary of hematite is highly coherent.

The lattice fringes originating from planes which are common to both hematite twins (*4*) and to goethite and hematite (Figs. 4, 5) look coherent. It thus seems that the array of oxygen atoms is not seriously fragmented or perturbed during transformation. However, we do not know whether the oxygen lattice is preserved perfectly apart from the rearrangement of Fe^{3+}. Both oxygen and iron might be rearranged, hematite crystallizing topotactically on goethite, i.e., in a local space, keeping the orientation relationship.

Continuing the creation of void–hematite units, the transformation progresses spatially with time at the transformation temperature. The progress of the reaction front is conditioned by the creation of new surface as a result of the formation of voids leading to the exposure of new goethite regions. Because the goethite surface at the transformation temperature is unstable, it transforms into hematite by the dehydration reaction. The reaction starts preferentially at places where the surface area per unit volume is largest, such as edges, surface steps, and crevasses in cleavage. When goethite is shielded from the surface, for example, surrounded by hematite or other films such as an amorphous carbon film, as in the case of Fig. 8, goethite is stable up to higher temperatures. The transformation is schematically summed up in Fig. 3.

After the specimen is completely transformed, grain growth of hematite crystallites begins on continued heating. This is a process of recrystallization performed by surface diffusion and coalescence, the contribution of bulk diffusion being presumably negligible. For example, in the case of synthetic goethite the transformation in air occurs at about 250°C and grain growth begins at just above that temperature (*9*). At such a low temperature, the diffusivity of Fe^{3+} (*14*) and O^{2-} (*15*) in bulk hematite is too small for grain growth.

The voids formed in this way play several roles (Fig. 3). They result from dehydration and promote the reaction by creating a new surface along which goethite is directly ex-

posed. A void works also as a path for the escape of water molecules. If these functions are blocked, the voids swell under the pressure of heated water vapor and goethite is shielded from the surface by hematite. Further reaction is impeded and the inside goethite remains stable, as observed in Fig. 8.

The regular periodic texture of hematite typically produced in vacuum has a very large specific surface area. Although hematite is the most stable among the Fe oxides, this special morphology keeps the product still in a high energy state, because much energy is stored as surface energy. This is the main driving force for further changes of morphology leading to forms with less surface area.

We now briefly describe the sequence of transformations and successive occurrences according to the present interpretation in comparison with the previous one, using Fig. 7.

The previous interpretations (*1, 16*) postulated the existence of donor and acceptor regions. The diffusion of protons was assumed to occur from the acceptor region to the donor region and that of iron in the opposite direction. The region with striae (Fig. 7a,b) was interpreted as an intermediate state formed by periodic changes of the iron atomic concentration in the oxygen atom array, on the way to the transformation into hematite (case (b) in 3.1). The diffusion away from iron atoms and the loss of oxygen by the formation of water molecules causes the donor region to finally become pores and the reaction is completed at this state (Fig. 7,c).

In the present explanation, the region with striae in Fig. 7a already represents the final product of a direct reaction. The progress from Fig. 7b to 7c results from changes in morphology by the recrystallization of hematite. The pores in Fig. 7c are the result of the growth of smaller voids.

4. Conclusions

Although it is difficult to obtain chemical information and quantitative data concerning reaction kinetics, high resolution electron microscopy is particularly powerful for obtaining information about the transformation mechanism. The present study has illustrated this in detail.

The reaction proceeds directly from oxyhydroxide to oxide in such a way that the reaction is completed in a local space of about 60 Å width; it consists almost exclusively of a nucleation stage with no lateral growth of oxide. This transformation first occurs at the surface. Spatial development of the bulk transformation proceeds by repeating the creation of void–hematite units resulting in a regular periodic texture. After transformation, the initial oxyhydroxide single crystal becomes a polycrystalline aggregate of twin related crystallites. This recrystallizes to form larger oxide grains as well as pores by surface diffusion and coalescence, thus releasing surface energy.

In this way the surface plays a key role for both transformation and the following recrystallization processes. The role of the voids is to create new surface and in this way allow the progress of the dehydration reaction into the bulk oxyhydroxide.

Under a partial pressure of water, goethite remains stable at temperatures where the transformation occurs in vacuum or under low partial pressure of water. Goethite might become unstable at higher temperatures where the bulk diffusivity of hydrogen and Fe^{3+} increases. This may affect the transformation mechanism. High resolution observations under a controlled atmosphere are necessary to solve this problem.

Acknowledgments

One of us (F.W.) acknowledges the fellowship awarded him by the Belgian Ministry of National Education (1976–1978). He is greatly indebted to Dr. J. C.

Mutin (University of Dijon) for useful discussions. He also appreciates the continuous encouragements of Professor N. Igata (University of Tokyo). The present study owes a great deal to the work done by Dr. J. Lima-de-Faria (laboratory TFQMP (*1*)) in its development. The authors express their thanks to him for his valuable comments and discussions.

References

1. J. LIMA-DE-FARIA, *Z. Kristallogr.* **119,** 176 (1963).
2. J. LIMA-DE-FARIA, *Acta Crystallogr.* **23,** 733 (1967).
3. J. R. GÜNTHER AND H. R. OSWALD, *Bull. Inst. Chem. Res. Kyoto Univ.* **53** (2), 249 (1975).
4. F. WATARI, J. VAN LANDUYT, P. DELAVIGNETTE, AND S. AMELINCKX, *J. Solid State Chem.* **29,** 137 (1979).
5. F. WATARI, P. DELAVIGNETTE, AND S. AMELINCKX, *J. Solid State Chem.* **29,** 417 (1979).
6. F. WATARI, *in* "Modulated Structures 1979," p. 385, AIP Conference Proceedings, No. 53, American Institute of Physics, New York (1979).
7. N. F. M. HENRY AND K. LONSDALE, *in* "International Tables for X-ray Crystallography," Vol. 1, p. 21, The Kynoch Press, Birmingham, England (1959).
8. F. WATARI, "Accuracy in Powder Diffraction," NBS Special Publication 567, p. 559, NBS, Gaitherburg (1979).
9. F. WATARI, J. VAN LANDUYT, P. DELAVIGNETTE, S. AMELINCKX, AND I. IGATA, *Phys. Stat. Sol.* (A) **73,** 215 (1982).
10. J. LIMA-DE-FARIA AND M. O. FIGUEIREDO, *J. Solid State Chem.* **16,** 7 (1976).
11. J. C. NIEPCE, M. T. MESNIER, AND D. LOUER, *J. Solid State Chem.* **22,** 341 (1977).
12. J. C. NIEPCE, Thesis, University of Dijon (1976).
13. J. M. COWLEY, *in* "Diffraction Physics," North–Holland, Amsterdam (1975).
14. W. C. HAGEL, *J. Amer. Ceram. Soc.* **48,** 70 (1965).
15. W. D. KINGERY, D. C. HILL, AND R. P. NELSON, *J. Amer. Ceram. Soc.* **43,** 473 (1960).
16. M. C. BALL AND H. F. W. TAYLOR, *Mining Mag.* **32,** 754 (1961).